



# Atomic cluster-structure calculations of the X-ray near-edge absorption of silver

E.C. Cosgriff, C.T. Chantler\*, C. Witte, L.F. Smale, C.Q. Tran

*School of Physics, University of Melbourne, Victoria 3010, Australia*

Received 23 February 2005; received in revised form 22 April 2005; accepted 6 June 2005

Available online 13 June 2005

Communicated by B. Fricke

## Abstract

A development of the finite difference method is used to compute atomic-cluster absorption spectra. The spectra is compared with recent high-precision measurements of the X-ray mass absorption coefficient of silver in the X-ray absorption fine structure region. The comparison indicates that in the near-edge region the finite difference method reproduces the fine structure qualitatively. The dominant theoretical techniques currently used in the literature to model these systems are the muffin-tin approach, the discrete variational method, the full linear augmented plane-wave approach and the finite difference method for near-edge structure. This Letter concentrates on the finite difference method and finds that this can be extended to the dominant XAFS regime successfully. In most investigations, amplitudes and energy scaling allow apparently good agreement of theory to be obtained with experiment. However, on absolute scales this comparison becomes weaker. This Letter relates to experimental data measured on an absolute scale to high accuracy, and therefore reveals both considerable agreement but also particular areas of discrepancy. Remaining discrepancies between theory and experiment relating to edge height, relative peak amplitudes and widths are discussed and invite further study.

© 2005 Elsevier B.V. All rights reserved.

PACS: 78.70.Dm; 61.10.Ht; 78.20.Bh; 32.80.Fb

Spectroscopy has become a widely used technique capable of delivering local structural information and revealing various electronic properties of the material under investigation. It has become an essential tool in

scientific fields such as materials science [1] and biophysics [2], requiring reliable theoretical simulations to enable detailed spectroscopic analysis.

X-ray absorption spectroscopy from inner-shell electrons is invaluable in this regard. The fine structure in the absorption spectra is a unique signature of the material, encapsulating detailed atomic, electronic and vibrational properties of the specimen. Advances

\* Corresponding author.

E-mail address: [chantler@ph.unimelb.edu.au](mailto:chantler@ph.unimelb.edu.au) (C.T. Chantler).

in experimental techniques, including the use of intense synchrotron X-ray sources, have made possible the extraction of these details to a high level of precision.

The extended region of X-ray absorption spectroscopy (above about 50 eV from the threshold) has been well explained qualitatively from the point of view of higher-order multiple scattering theory. However, major anomalies exist, several keV or even 40% above the edge energy, even for very well understood materials [3–5]; other anomalies exist in the intermediate extended region above the absorption edge.

Significant progress has recently been made in the theoretical development of X-ray absorption spectroscopy in the fine structure region of the edge. Progress in understanding the near-edge region has been slower due to the difficulty of accurate normalisation and of correctly accounting for many-body effects including shake-up and shake-down processes, the core hole and inelastic scattering. The past three decades have seen a number of advances in the ability to calculate X-ray absorption near-edge structure (XANES) spectra, resulting in a range of ab initio computer codes. Approaches include band structure calculations, cluster methods and path-by-path techniques. Common cluster models use the  $X_\alpha$  scattered wave method [6,7], which invokes the muffin-tin approximation to the potential. Alternatively, one can use the discrete variational method [8] or the finite difference method for near-edge structure (FDMNES) [9]. The latter approaches avoid the muffin-tin approximation, but are limited to low-energy calculations. Recent developments of the FDMNES method have been applied to a range of applications in a useful manner [10–13]. The full linear augmented plane-wave approach [14] is also independent of the muffin-tin approximation but is limited to structures where a periodic potential is applicable.

Across the range of current theoretical and experimental results, numerous inconsistencies have been reported [5,11,12,15–17]. The X-ray mass absorption coefficient of silver was recently measured using the X-ray extended range technique with an accuracy of 0.27%–0.4% including the accuracy of both energy and absorption determination [18]. This unprecedented level of accuracy in experimental results (by a factor of 4–10 over all previous observations of silver) provides an opportunity to probe atomic and solid state

wave function calculations. This Letter will examine the applicability of the finite difference method to the case of silver. It is the first application of the FDMNES approach which has been extended from the near-edge XANES region to enable investigation of the dominant structure of the XAFS processes and the oscillations further away from the edge. We believe that some key issues of interpretation can only be addressed by this extension of range of theoretical computation.

A brief outline of the finite difference method theory will be given here, the full treatment can be found in [9].

The photoabsorption cross section is given by

$$\sigma = 4\pi^2\alpha\hbar\omega \sum_{f,g} |M_{fg}|^2 \delta(\hbar\omega - E_f + E_g), \quad (1)$$

where  $\alpha$  is the fine structure constant,  $\hbar\omega$  is the photon energy and  $E_g$  and  $E_f$  are the respective energies of the initial and final states. Neglecting spin, the transition matrix elements are given by

$$M_{fg} = \langle \psi_f | \boldsymbol{\epsilon} \cdot \mathbf{r} e^{i\mathbf{k}\cdot\mathbf{r}} | \psi_g \rangle, \quad (2)$$

where the photons have a wave vector  $\mathbf{k}$  and are polarized in the  $\boldsymbol{\epsilon}$  direction. The initial core state is given by  $\psi_g$  and  $\psi_f$  is the final-state wave function. The program allows for an expansion of the exponential up to third order—the octupole term. The real component of the form factor (i.e., the transform of the imaginary component) is usually more affected by the relativistic corrections to the wave function, partially revealed by the high-order multipoles [16,17].

The time independent Schrödinger equation is solved on a discrete set of lattice points [19], a method which is computationally expensive. The Laplacian is approximated by a polynomial of order four, this order being more economical than the second-order polynomial. The accurate calculation of the final-state wave function has proved to be elusive and this is the main aim of the FDMNES approach. As no approximations are made about the shape of the potential, problems associated with the muffin-tin approach, such as neglecting warping effects, are eliminated. The muffin-tin approximation is noted to be inadequate in the XANES regime [20], although qualitative agreement has been obtained recently in a number of cases using muffin-tin approaches [21]. The assumption made about the charge density and thus the potential being constant in the interstitial region leads to discrepancies

in the simulated spectra. It is in this region that the finite difference method is employed. The local density approximation is used to calculate the potential surrounding the absorbing atom in the cluster, with the electronic densities being calculated independently. A first approximation is to take a superposition of atomic densities which is then modified for bonding effects and dilated orbitals. An appropriate choice of occupied orbitals is necessary for an accurate representation of the potential. The final-state rule is used when constructing the scattering potential; the charge density is calculated using the initial specified configuration with an appropriate core–hole and the extra electron in the lowest lying unoccupied state. This method is noted to be suitable for low-energy XAFS, with a fully relaxed ‘primary channel’ [20].

The calculation is divided into three regions: the atomic core, the interstitial and the outer sphere. The atomic core is assumed spherically symmetric and expanded in spherical harmonics  $Y_L$  as

$$V(\mathbf{r}) = \sum_L V_L(r) Y_L(\Omega). \quad (3)$$

The radial distance from the centre of the atom is  $\mathbf{r} = (r, \Omega)$ . The angular momentum and azimuthal quantum numbers are denoted by  $L = (l, m)$ . The atomic sphere is smaller than a typical muffin-tin sphere. Independent solutions to the Schrödinger equation are used to express the general solution in the atomic sphere as

$$\psi(\mathbf{r}) = \sum_L a_L \phi_L(\mathbf{r}). \quad (4)$$

A set of coupled differential equations is solved for the independent solutions  $\phi_L(\mathbf{r})$ . Amplitudes  $a_L$  and the wave function in the interstitial region are solved by imposing continuity across the boundary. In the outer sphere, the final-state wave function is connected to the continuum by expanding it in terms of generalised Neumann and Hankel functions where the amplitudes  $\tau_L$  are again to be solved via coupling with the finite difference method grid:

$$\psi_f = J_L(\mathbf{r}) + i \sum_L \tau_L H_L^{(1)}(\mathbf{r}). \quad (5)$$

The potential in the outer sphere is assumed to be constant or at least spherically symmetric.

Calculations were performed for the  $K$ -edge of silver with cluster radii of 5 and 7 Å. This corresponds to 19-atom and 79-atom clusters, respectively. An inter-point distance of  $h = 0.25$  Å was used, giving rough estimates of 32 000 points in the FDM grid for the 5 Å cluster and 66 000 points for the larger 7 Å cluster. As expected, a significant amount of CPU time was required for these calculations and a 7 Å calculation could take several days. The maximum angular momentum used when matching to the continuum, is given by

$$kr = \sqrt{l_{\max}(l_{\max} + 1)}, \quad (6)$$

where  $k$  is the photoelectron wave vector and  $r$  is the cluster radius. Atomic wave functions were calculated self-consistently using a fully relativistic Dirac–Slater model. The cross section is given as the sum of atoms equivalent by symmetry and must be normalised appropriately after computation. The details of the experiment are available in the published paper [18], but the experiment was performed at room temperature.

The matrix elements were calculated in the dipole approximation. One octupole expansion calculation was performed for a 5 Å cluster in order to investigate contributions to the matrix element from higher-order relativistic terms. It was anticipated that dominant effects would be seen in the real component of the form factor (not directly measured in these experiments) or localised in the mass absorption coefficient (and the imaginary component of the form factor). The dipole and octupole results were indistinguishable, indicating that local effects in the region of interest were not important, and hence that in this sense the calculation had converged.

Investigations revealed that the FDMNES code computed the atomic density using an initial electronic configuration of  $[\text{Kr}]4d^9 5s^2$ . The code is not a single-configuration code but nonetheless adopts the symmetry of the nominated configuration. As this choice has direct consequences for the atomic and cluster potentials, the code was rewritten to repeat the computation using an electronic configuration of  $[\text{Kr}]4d^{10} 5s^1$ . This configuration shifts the energy of the initial state by 4.263 eV. The results for a 7 Å cluster are shown in Fig. 1. This is a useful but minor modification of the core basis set. The change is consistent with the shifting of one valence electron, representing one 47th of the charge and a minimal binding contribution in

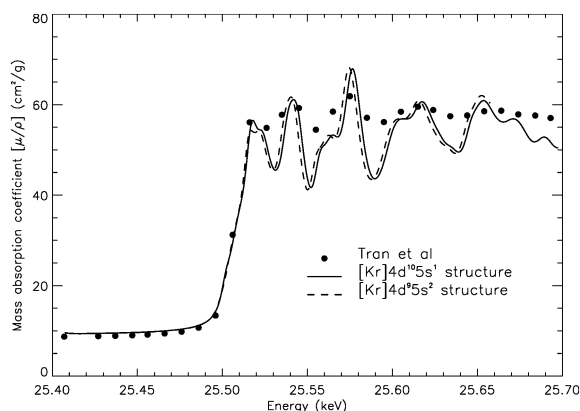


Fig. 1. Detail of near-edge oscillations showing comparison with theoretical predictions from FDMNES. The circles are the absolute mass absorption coefficients of [18]. The experimental data has an accuracy of 0.39%–1.14%, approximately the size of the circles. Predictions are for two different initial electronic configurations, convolved with a Lorentzian of width 6.42 eV. The cluster radius is 7 Å.

the region of the core (*K*-shell) electron. Although a more elaborate multi-configurational Dirac–Fock wave function may show different quantitative behaviour, the scale of expected shifts is indicated by this comparison and is quite inadequate to explain structural features not addressed by either computation. The qualitative conclusions of this work are therefore unaffected by this detail.

Convergence was investigated by comparing the results from different cluster sizes. Fig. 2 shows the results from a single atom and from the 5 and 7 Å clusters. The results from the larger cluster are expected to be a better fit as the photoelectron experiences a larger number of scattering events inside the cluster. Convergence is reached for the 7 Å cluster. However, as the spectra shown here are for a single broadening parameter, only the edge region is matched.

Lifetime and experimental broadening effects are not included in the FDMNES code and must be taken into account after the calculation. The choice of broadening processes and parameters ultimately affects the agreement between theory and experiment. The spectrum shown in Fig. 1 was convolved with a Lorentzian of width 6.42 eV. Previously reported results for the hole width are within the range of 6.28 to 7.90 eV [22–24] (the Lorentzian width is inversely proportional to the *K*-shell lifetime).

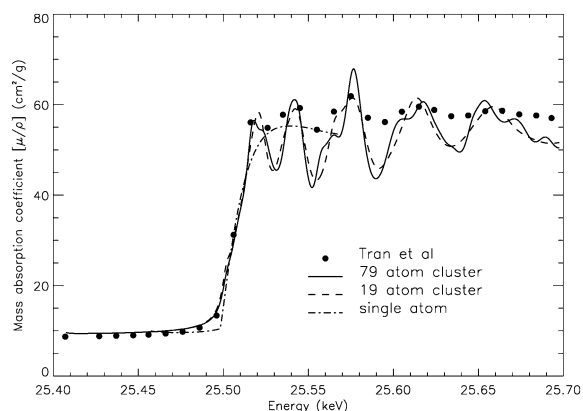


Fig. 2. Detail of the near-edge oscillations on an absolute scale showing comparison with increasing cluster size. The circles are the absolute mass absorption coefficients of [18]. In this figure and in all computations, the edge height does not agree with the experimental result.

The results agree well in the region of the edge although two offsets are required. The calculated spectra were shifted by 6.54 eV and a background level of 8 cm<sup>2</sup>/g was added when comparing experimental results with the calculated total mass absorption coefficient. As the computation relates solely to the ionization of the *K*-shell electron, a background level for the contributions of photo-ionization from *L* and *M* shells needs to be added. The contribution from scattering processes to the measured absorption coefficient is negligible and is discussed in [18]. It is clear that the hole width underestimates the various lifetime effects and other contributing widths, as the calculated spectrum is still sharply peaked compared to the experimental result. While the energy positions of the peaks are fairly well predicted, relative amplitudes are underestimated.

The nominal hole (or Lorentzian) width was then increased in an attempt to obtain agreement between the theory and experiment above the edge. The first three peaks are matched when the spectrum is broadened with an unphysical hole width of 14.0 eV but the next two require a surprisingly large width of 30.0 eV to obtain qualitative agreement with the observed structure and widths. However, in the process of increasing the width, the edge-jump and near-edge structure show strong (violent) discrepancies from the experimental data.

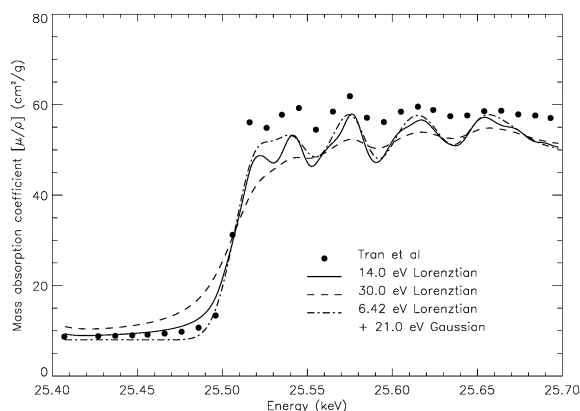


Fig. 3. The effect of possible theoretical and experimental broadening. The circles are the absolute mass absorption coefficients of [18]. The solid line is the result of Lorentzian broadening with a 14.0 eV width; the dashed line, a Lorentzian with a 30.0 eV width. The dash-dot line is the result of Lorentzian broadening with a 6.42 eV width and subsequent Gaussian broadening with a 21.0 eV width.

The results are shown in Fig. 3: this purely Lorentzian broadening does not lead to an acceptable interpretation of the data. Fig. 3 also shows a theoretical spectrum broadened with a Lorentzian of width 6.42 eV and a Gaussian of width 21.0 eV in order to simulate additional experimental broadening of a possibly different character. Slit (i.e., top hat), Gaussian broadening or convolutions of these mimic most experimental broadening processes. However, these also fail to agree with the experimental results, being too broad for the near-edge peaks and too sharp for the far-edge oscillations. Therefore, this indicates that experimental broadening processes have already been correctly dealt with in the experimental analysis and are not dominant in this comparison to theory. In fact, the literature values of the hole width appear approximately correct in matching the edge region. Final-state broadening is energy-dependent and would be expected to at least broaden the oscillations, as the different onset energies for a particular channel will vary the relative phase for each channel at a given energy. However, this could yield increased broadening above the edge, but would not continue to broaden the theoretical prediction as observed.

The coherence of the beam has been claimed to be a major contributor to the XAFS oscillation amplitudes, and this of course depends upon the size of the synchrotron ring, the exit slit width and hence the trans-

verse coherence of the X-ray source [25]. We agree that the observation of speckle, of diffraction fringes in crystallographic experiments, and similar effects are completely dependent upon the synchrotron source coherence [26–28]. Transverse beam coherence is however not a likely contributor to XAFS oscillations as the process is dominated by the interference between an emerging photoelectron wave and a returning wave. Hence the relative phase along this path should be of sole importance and not the absolute phase of the incident X-ray beam.

The disagreement could be ascribed to structural imperfections, grain boundaries and mosaicity of the silver specimens used. This functional form might be able to explain the discrepancy, but quantitatively the silver experiment should be dominated by the bulk behaviour of the material.

A more likely cause for the discrepancy observed in shape and broadening could be the thermal vibration of the bound electrons of atoms, leading to a Debye–Waller thermal smearing of the XAFS structure, especially for oscillations further above the edge. Then the relative phase of the path is not uniform from one X-ray absorption to the next, or from one atomic site to the next, and the interfering wave undergoes decoherence so the oscillations are damped. Thermal effects in XANES and near-edge XAFS have previously been reported to be negligible [20,29]. As a result the FDMNES code performs a ‘frozen cluster’ calculation, with no allowance for Debye–Waller factors.

The mean amplitude of vibration of a silver atom is reported as  $\sigma = \sqrt{\langle u^2 \rangle} = 0.173 \text{ \AA}$  [30]. The second peak in the above-edge structure is approximately 25 eV above the edge, corresponding to a wave vector  $k = 2.56 \text{ \AA}^{-1}$ . This leads to a simple estimate of the damping of the amplitude of the third peak above the edge of  $e^{-2\sigma^2 k^2} = 0.68$ . Even for the third peak alone, 69 eV above the edge, this would lead to a damping of the amplitude by a factor of 0.34. Correlated (bonding) amplitudes of vibration can be far smaller than the quoted figures (for particular orbitals) but in that case this postulated cause is even less able to explain the features observed. The development of broadening in the real (high-resolution) data as a function of energy above the edge is very pronounced even within the first two or three peaks above the edge. Hence this broadening (which is certainly partially thermal or Debye–

Waller in nature) has already become significant by the second peak—which conventionally implies that this thermal broadening is indeed already visible in the XANES region.

As opposed to the earlier literature, the results obtained here would imply that thermal effects in these near-edge regions are actually quite significant. Such broadening has been observed at high temperatures in silver [20]. This furnishes a plausible explanation of qualitative differences between theory and experimental data, but the magnitude of the resulting damping appears insufficient to account fully for the discrepancy. Disorder (thermal or other) effects are always taken into account in current EXAFS analysis. However, this is not the case for FDM techniques in the XANES region. Several recent papers have used or developed the FDM approach successfully in application to XANES [11–13]. Perhaps the surprising issue is not that these are needed in the range of our experimental comparison, but that they appear insufficient.

Developments of the muffin-tin approach have been used with success in the near-edge region [21]. Their Fig. 3 is a lovely exposition of distortions in geometry and the consequent impact upon the XANES spectrum. The current work develops and challenges the FDM approach over a wider region, but notes that recent work with muffin-tin approaches also has similar qualitative difficulties. In particular, [21] claims good agreement, and has clear qualitative success, but also has the same problems of detailed agreement of amplitudes in the XAFS region, as illustrated in their Fig. 2.

The Dirac–Slater method used for the calculation of wave functions has a number of difficulties, including the inadequate treatment of continuum and excited states. An extended basis method might, if carefully implemented with judicious inclusion of level widths and thermal motion, alleviate some of these difficulties. The main difficulty is in the representation of the exchange correlation potential. Recent advances made with relativistic density functional theory [31] might yield a more effective treatment of the exchange correlation contribution.

The high degree of symmetry and close packing of silver implies that a muffin-tin approximation could be reasonably justified in this case, and that these calculations might also provide a useful comparison. Other studies with a 13-atom copper cluster suggest that the more conventional muffin-tin approaches may be

quite applicable and show similar insight in a related regime.

However, this method retains specific details about the interstitial potential, a significant advantage when dealing with targets of low-symmetry. It is computationally difficult to extend the FDMNES code from the XANES region and future prospects are limited by available hardware and CPU time. The maximum  $l$  value when connection between the outer sphere and the grid is made is obtained via Eq. (6), so the angular momentum basis set increases towards higher energies. As the final-state matching is performed using an expansion in spherical waves, more spherical harmonics are needed, thus  $l_{\max}$  must increase. As the photoelectron energy increases and hence  $k$ , that so too may the cluster radius in order to ensure an accurate representation of the continuum wave function. This then extends computational time due to the larger number of FDM points in the grid. While the method has raised questions here regarding hole-widths, thermal effects and XAFS widths, it is clear that the structure can be probed more critically with this level of experimental data and this extended approach of FDM. This method has proved to be very suitable for exploring the boundary between XANES/EXAFS.

We have demonstrated that the FDMNES routine is relevant and useful in the near-edge region and have extended the approach into the XAFS region. Lifetime broadening effects need to be included together with an energy offset, a correction to the background level, an apparent adjustment of the edge-jump, and a thermal Debye parameter to improve agreement between theory and experiment. Nonetheless, further improvement will be required, inviting future experimental and theoretical investigations.

## Acknowledgements

The authors acknowledge collaborators at the Advanced Photon Source and especially M.D. de Jonge and Z. Barnea, and thank Y. Joly for assistance in access to and implementation of the FDMNES approach. This work was supported by the Australian Synchrotron Research Program, funded by the Commonwealth of Australia under the Major National Research Facilities Program, and by the Australian Research Council. Use of the Advanced Photon Source

was supported by the US Department of Energy, Basic Energy Sciences, Office of Energy Research, under Contract No. W-31-109-Eng-38.

## References

- [1] T.C. Rojas, et al., *J. Mater. Sci.* 39 (2004) 4877.
- [2] M. Benfatto, et al., *Biophys. Chem.* 110 (2004) 191.
- [3] C.T. Chantler, Z. Barnea, *J. Phys.: Condens. Matter* 11 (1999) 4087.
- [4] C.Q. Tran, C.T. Chantler, Z. Barnea, *Phys. Rev. Lett.* 90 (2003) 257401.
- [5] N.K. Del Grande, *SPIE Proc.* 691 (1986) 2.
- [6] K.H. Johnson, *Adv. Quantum Chem.* 7 (1973) 143.
- [7] F.W. Kutzler, et al., *J. Chem. Phys.* 73 (1980) 3274.
- [8] D.E. Ellis, G.L. Goodman, *Int. J. Quantum Chem.* 25 (1984) 185.
- [9] Y. Joly, *Phys. Rev. B* 63 (2001) 125120.
- [10] Y. Joly, S. Di Matteo, C.R. Natoli, *Phys. Rev. B* 69 (2004) 224401;  
G.E. Tommei, F. Baletto, R. Ferrando, R. Spadacini, A. Danani, *Phys. Rev. B* 69 (2004) 115426;  
A. Bombardi, J. Rodriguez-Carvajal, S. Di Matteo, F. de Bergevin, L. Paolasini, P. Carretta, P. Millet, R. Caciuffo, *Phys. Rev. Lett.* 93 (2004) 027202.
- [11] P. D'Angelo, M. Benfatto, S. Della Longa, N.V. Pavel, *Phys. Rev. B* 66 (2002) 064209.
- [12] Z.Y. Wu, D.C. Xian, et al., *Phys. Rev. B* 70 (2004) 033104.
- [13] S. Di Matteo, Y. Joly, A. Bombardi, et al., *Phys. Rev. Lett.* 91 (2003) 257402.
- [14] P. Blaha, R. Schwarz, P. Sorantin, S. Trickey, *Comput. Phys. Commun.* 59 (1990) 399.
- [15] C.T. Chantler, et al., *Phys. Lett. A* 286 (2001) 338.
- [16] C.T. Chantler, *J. Phys. Chem. Ref. Data* 24 (1995) 71.
- [17] C.T. Chantler, *J. Phys. Chem. Ref. Data* 29 (2000) 597.
- [18] C.Q. Tran, et al., *J. Phys. B: At. Mol. Opt. Phys.* 38 (2005) 89.
- [19] G.E. Kimball, G.H. Shortley, *Phys. Rev.* 45 (1934) 815.
- [20] J.J. Rehr, R.C. Albers, *Rev. Mod. Phys.* 72 (2000) 621.
- [21] O. Siper, G. Dalba, F. Rocca, *Phys. Rev. B* 69 (2004) 134201.
- [22] J.H. Scofield, *At. Data Nucl. Data Tables* 14 (1974) 121.
- [23] V.O. Kostroun, M.H. Chen, B. Crasemann, *Phys. Rev. A* 3 (1971) 533.
- [24] E.J. McGuire, *Phys. Rev. A* 3 (1970) 273.
- [25] J. Hunter Dunn, D. Arvanitis, R. Carr, N. Mårtensson, *Phys. Rev. Lett.* 84 (2000) 1031.
- [26] I.K. Robinson, et al., *Phys. Rev. B* 52 (1995) 9917.
- [27] J. Lin, et al., *Phys. Rev. Lett.* 90 (2003) 074801.
- [28] D. Paterson, et al., *Opt. Commun.* 195 (2001) 79.
- [29] N. Dimakis, G. Bunker, *Phys. Rev. B* 58 (1998) 2467.
- [30] N.M. Butt, J. Bashir, B.T.M. Willis, G. Heger, *Acta Crystallogr. A* 44 (1988) 396.
- [31] S. Varga, et al., *J. Chem. Phys.* 112 (2000) 3499.